Simulation Study for the Ceramic Powder Compaction Proces

Omed Gh. Abdullah[(a)], Fadhil Abd Rasin[(b)] , and Tariq A. Al-Dhahir[(c)]
(a) Sulaimani University, College of Science, Physics Department
(b) Al-Mustansiriya University, College of Science, Physics Department
(c) Baghdad University, Iben al-Haithem College, Physics Department

Abstract

The accurate simulation of powder compaction involves many different areas in computational mechanics, where appropriate elastoplastic constitutive model, finite deformation framework, enforcement of contact, friction conditions and robust numerical methods are some of the requirements demanded in this simulation. The modified Drucker-Prager Cap (DPC) elasto-plastic constitutive model is used for the calculations that performed using the finite element code ABAQUS 6.4, to simulate densification of alumina powder using cold die pressing. A comparison of the experimental and theoretical density distribution shows that there is a good qualitative agreement in the sense that both produce the important maximum and minimum density regions accurately, despite the overall density distribution of present work is slightly underestimated experimental data.

Introduction:

In recent decades, a substantial amount of research and development has been conducted in different areas and significant technological advances have been made. Scientists have been trying to find appropriate models that can describe the characteristics of different kinds of powders and predict the behaviors of the powder precisely during the manufacturing process for the industry. It is of great significance because this will bring more economic effects to the industry and engineers can control the particle compaction [1].

One of the most important production routes for powder metal or ceramic parts is uniaxial die pressing and sintering. Although complex parts can be produced but it is not possible to achieve a homogeneous green density distribution by die compaction [2]. The more or less inhomogeneous in density is depending on the; part geometry, the tool design and the friction between powder and die wall. Since the part undergoes shape distortions during sintering, or cracks may develop, and the correction of shape distortions by hard machining is expensive and the tolerance requirements are often extremely high, it may be a costly and time-consuming process to find a tool design and a pressing schedule giving good parts within the required tolerances, so the alternative way is to optimize the process by computer simulation [3,4].

Modified Drucker-Prager/Cap Model:

The yield surface of the modified Drucker-Prager/Cap plasticity model includes two main segments: A shear failure surface, providing dominantly shearing flow, and a "cap," which intersects the equivalent pressure stress axis (Fig.1) [5]. Inside the yield surface, the powder behaves elastically. If the stress state reaches the yield surface, the powder deforms plastically [6]. The density increases, if the stress state is on the cap, whereas it decreases (dilatation), when the stress state reaches the failure line. Dilatation implies softening, so that strain localization and cracking may occur.

There is a transition region between these segments, introduced to provide a smooth surface. The cap serves two main purposes: it bounds the yield surface in hydrostatic compression, thus providing an inelastic hardening mechanism to represent plastic compaction, and it helps to control volume dilatancy when the material yields in shear by providing softening as a function of the inelastic volume increase created as the material yields on the Drucker-Prager shear failure and transition yield surfaces [7].

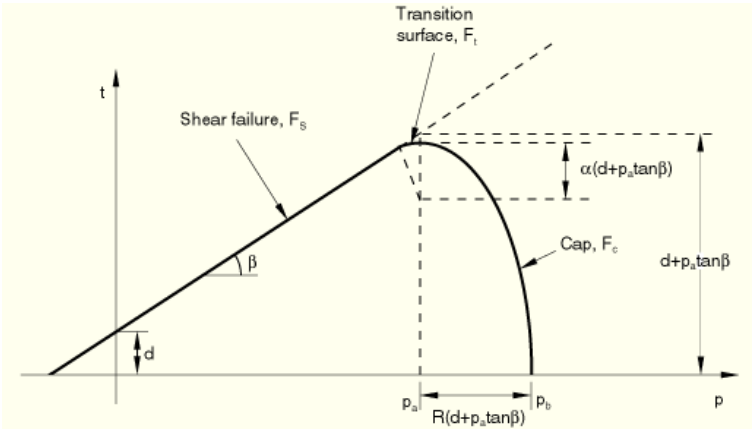

Fig.1: Modified Drucker-Prager/Cap model: yield surfaces in the p-t plane [5].

The model uses associated flow in the cap region and non-associated flow in the shear failure and transition regions.

The linear strain rate decomposition for time independent is assumed, so that

$$d\varepsilon = d\varepsilon^{el} + d\varepsilon^{pl} \tag{1}$$

$$d\varepsilon = D^{el\,-1} d\sigma + d\lambda \frac{dG}{d\sigma} \tag{2}$$

where $d\varepsilon$ is the total strain rate, $d\varepsilon^{el}$ is the elastic strain rate, and $d\varepsilon^{pl}$ is the inelastic (plastic) time-independent strain rate. D^{el} is the elastic matrix, G is plastic potential and, $d\lambda$ denotes a proportionality constant termed the plastic multiplier. In equation (2) the elastic strain increment is related to the stress increment by the elastic matrix which depends only on the current state of stress.

The elastic stress-strain matrix D^{el} for isotropic axisymmetric materials is given from the generalized Hooke's law using the Young's modulus and the Poisson's ratio [8]:

$$D^{el} = \frac{E(1-\nu)}{(1+\nu)(1-2\nu)} \begin{bmatrix} 1 & \frac{\nu}{1-\nu} & 0 & \frac{\nu}{1-\nu} \\ \frac{\nu}{1-\nu} & 1 & 0 & \frac{\nu}{1-\nu} \\ 0 & 0 & \frac{1-2\nu}{2(1-\nu)} & 0 \\ \frac{\nu}{1-\nu} & \frac{\nu}{1-\nu} & 0 & 1 \end{bmatrix} \tag{3}$$

The yield surface for the Drucker-Prager/cap model is represented in Fig.1 [5]. It consists of F_s (the shear failure (yield) line), F_c (the cap yield curve) and F_t (a transitional yield curve for smoothening between F_s & F_c). The shear yield line [9] is:

$$F_s = q - (\tan\beta)p - d = 0 \tag{4}$$

where d is the material cohesion, and β is the material friction angle. The plastic flow along the shear failure line is non-associative. Plastic hardening occurs when the powder compact yields on the cap. As the material hardens, the cap curve expands gradually from the dashed curves to the solid curve as illustrated with a dashed arrow line in Fig.2. The shape of the cap is controlled by a shape factor R ($0<R<1$) and a transition parameter α (typically $0.01<\alpha<0.05$).

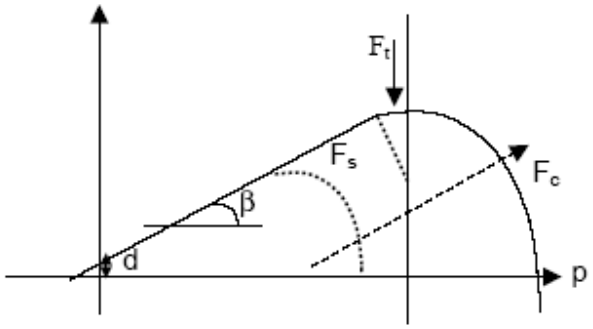

Fig.2: Schematic of flow for the modified Drucker-Prager/cap model in p-q space [10]

The cap surface hardens or softens as a function of the volumetric plastic strain, having two different effects, when yielding on the cap the volumetric plastic compaction causes hardening, while volumetric plastic dilation causes softening when yielding on the shear failure surface [11].

The cap yield surface has an elliptical shape and is written as [12]:

$$F_c=\sqrt{\left(p-p_a\right)^2+\left(\frac{Rq}{1+\alpha-\frac{\alpha}{\cos\beta}}\right)^2}-R\left(d+p_a\tan\beta\right)=0 \tag{5}$$

where p_a is an evolution parameter representing the hardening or softening driven by the volumetric plastic strain, and is given by:

$$p_a=\frac{p_b-Rd}{\left(1+R\tan\beta\right)} \tag{6}$$

where p_b is the hydrostatic pressure yield surface that defined the position of the cap. p_b is generally assumed be dependent upon the volumetric inelastic strain ε_{vol}^{in}, such that:

$$p_b=p_b\left(\varepsilon_{vol}^{in}\right)=p_b\left(\varepsilon_{vol}^{in}\big|_0+\varepsilon_{vol}^{pl}+\varepsilon_{vol}^{cr}\right) \tag{7}$$

where $\varepsilon_{vol}^{in}\big|_0$ is the initial volumetric plastic strain before compaction, ε_{vol}^{pl} is the plastic volumetric strain and ε_{vol}^{cr} is the creep volumetric strain. $\varepsilon_{vol}^{cr}=0$ is usually assumed in an elastic-plastic problem. The typical cap hardening is shown in Fig.3:

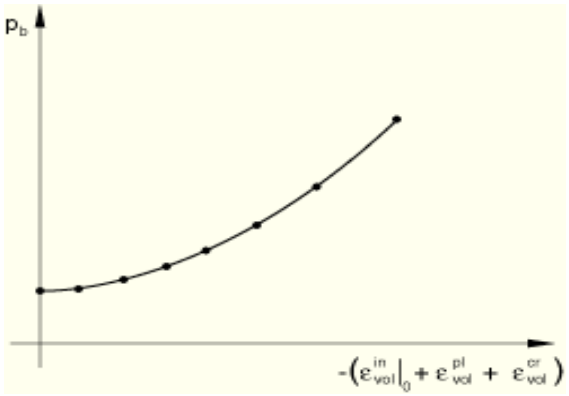

Fig.3: Typical Cap hardening [5].

In order to ensure that the primary feature of the DPC model is not significantly modified by the introduction of the transition segment for the sake of numerical implementation, the transition segment is always relatively small by restricting the parameter α [13]. The transition yield line is described as:

$$F_t = \sqrt{(p - p_a)^2 + \left[q - \left(1 - \frac{\alpha}{\cos\beta}\right)(d + p_a \tan\beta)\right]^2} - \alpha(d + p_a \tan\beta) = 0 \qquad (8)$$

where the hydrostatic pressure p, and effective stress q can be written as:

$$p = -\frac{1}{3}(\sigma_1 + \sigma_2 + \sigma_3) = -\frac{1}{3}(\sigma_1 + 2\sigma_2) \qquad (9)$$

$$q = -(\sigma_1 - \sigma_2) \qquad (10)$$

During the compaction, when the direction 1 is regarded as the axial direction and the direction 2,3 are regarded as the lateral directions, respectively, then $\sigma_2 = \sigma_3$ and $\varepsilon_2 = \varepsilon_3$ in the standard triaxial compression test [14].

Simulation Study:

Verification of the model is very important particularly when the material model is heavily dependent on experimental data. For this purpose, we adopt a compact geometry designed by Aydin et al [15], and Kim [16]. Our simulation results are compared with their experimental results. This comparison gives the confidence of the reliability of the model before proceeding to simulate other geometries of concern.

In the present work, a finite element analysis has been used to modeled the formation of compacted Alumina ceramic powder, during a simple compaction process. The analysis was performed using the finite element code ABAQUS 6.4, with modified Dracker-Prager Cap elasto-plastic constitutive model [5].

The numerical analysis of the die compaction process requires a consideration of three discrete parts, the compression mode, the unloading (removal of the upper punch) and the ejection (removal of the compacted component from the die). The loading is executed by incrementally increasing the punch displacement. The unloading and the ejection are executed by incrementally releasing the surface boundary traction developed during pressing.

The Drucker-Prager-Cap Parameters Determination:

Coube and Riedel [17] modify, Druker Prager Cap model to describe the powder behavior more realistically especially with respect to crack formation during pressing, unloading or ejection. By their modification they showed that not only the hardening function p_a, but also the cohesion parameters d, and material friction angle β should depend on the density. In the following relations, the density ρ and the volumetric plastic strain ε_{vol}^{pl} are alternatively used. They are related by

$$\varepsilon_{vol}^{pl} = \ln\left(\frac{\rho}{\rho_o}\right) \tag{11}$$

where ρ_o is the filling density. The hardening relation, the cap eccentricity and the cohesion parameters are described by the following empirical expressions [18]:

$$\varepsilon_{vol}^{pl} = W\left(1-\exp\left(-c_1 p_a^{c_2}\right)\right) \tag{12}$$

$$R = R_1 + R_2 \exp\left(R_3 \rho\right) \tag{13}$$

$$d = d_1 \exp\left(d_2 \varepsilon_{vol}^{pl}\right) \tag{14}$$

$$\tan\beta = b_1 - b_2 \varepsilon_{vol}^{pl} \tag{15}$$

where R is the Cap eccentricity, and the parameters W, c_1, c_2, R_1, R_2, R_3, d_1, d_2, b_1 and b_2 are determined from experiments data fitting.

For the compaction simulation, powder of 96 % purity alumina (Al_2O_3) were used. The numerical values of the cohesion and, hardening parameters, are give as $W = 0.84042$, $c_1 = 0.61894\,\text{MPa}$, $c_2 = 0.57469$, $R = 0.558$, $d_1 = 0.00877\,\text{MPa}$, $d_2 = 6.33035$, $b_1 = 2.2747$, and $b_2 = 0.09038$ [19]. The exact value of the cap eccentricity has an only minor influence on the final density distribution in many practical cases [20], so that the cap eccentricity is taken to be constant.

The fill density was assumed to be uniform in the simulation. The fill density (density of the compact before compaction) of alumina powder is $1.679\,gm/cm^3$ [16], and the theoretical density is $3.986\,gm/cm^3$. The transition surface parameter, α, is assumed to be 0.03 [5].

In this study, the cohesion parameter, and cohesion angle, are choose as a variable with respect to density, which differs from the approach of other studies which considers these parameter are constant during the compaction. The purpose behind this approach is to study the effect of there variability on the final result for alumina powder compaction.

The cohesion parameter (the interaction of the shear failure line with the effective stress axis) with respect to plastic volumetric strain are shown in the Fig.4, and the cohesion angle (slope of the failure line) behavior with respect to plastic volumetric strain are shown in Fig.5. The hardening parameters (p_a and p_b) are shown by the Fig.7 and Fig.8 respectively.

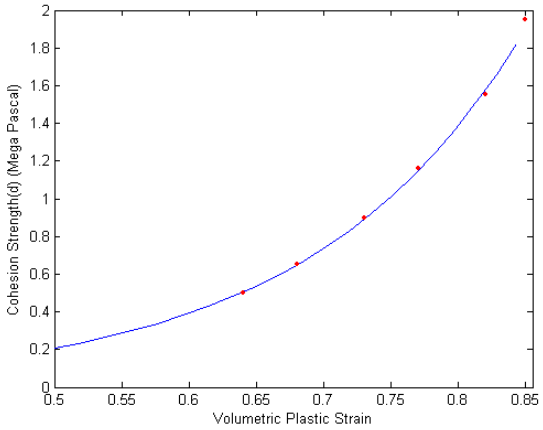

Fig.4: Cohesive strength d versus volumetric plastic strain for an alumina powder.

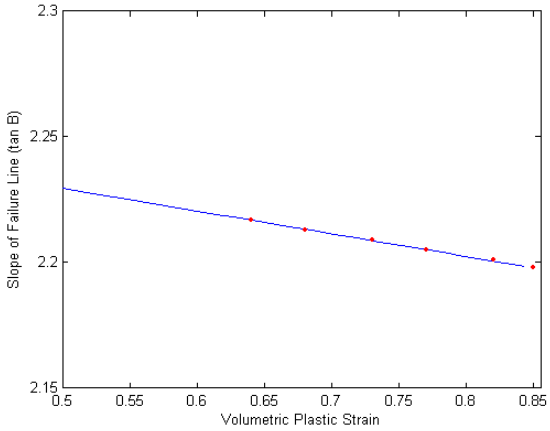

Fig.5: Slope of failure line versus volumetric plastic strain for an alumina powder.

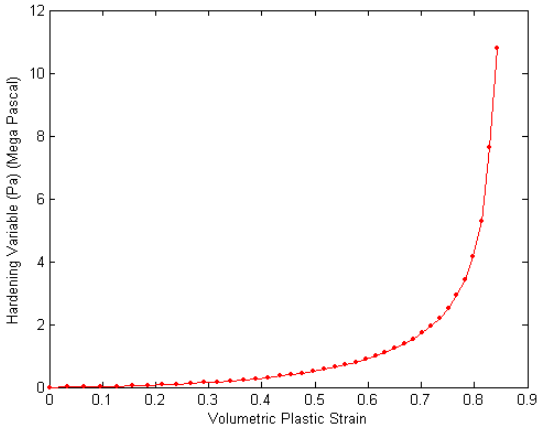

Fig.6: Volumetric plastic strain as function of hardening variable p_a, for an alumina powder.

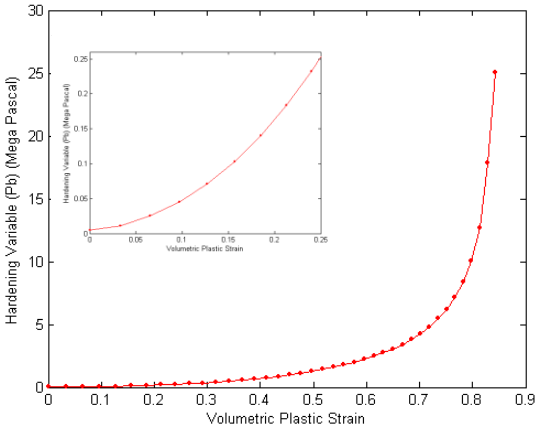

Fig.7: Hardening variable p_b versus volumetric plastic strain for an alumina powder.

By some transformation on the equations (5) and (8), these two equations can be obtained respectively, which can be used to obtain the behaviour of yield function of the alumina powder:

$$q = \frac{1}{R}\left(1+\alpha+\frac{\alpha}{\cos\beta}\right)\sqrt{\left[R\left(d+p_a\tan\beta\right)\right]^2-\left(p-p_a\right)^2} \qquad (16)$$

$$q = \alpha\left(d+p_a\tan\beta\right)+\left(1-\frac{\alpha}{\cos\beta}\right)\left(d+p_a\tan\beta\right) \qquad (17)$$

From these two equations and by putting $p = p_a$, the value of von mises stress can be obtained at p_a for two yields surfaces, and then the range of transition surface can be obtained, which is in the range $[p_a - AD, p_a + AD]$, as shown in Fig.8:

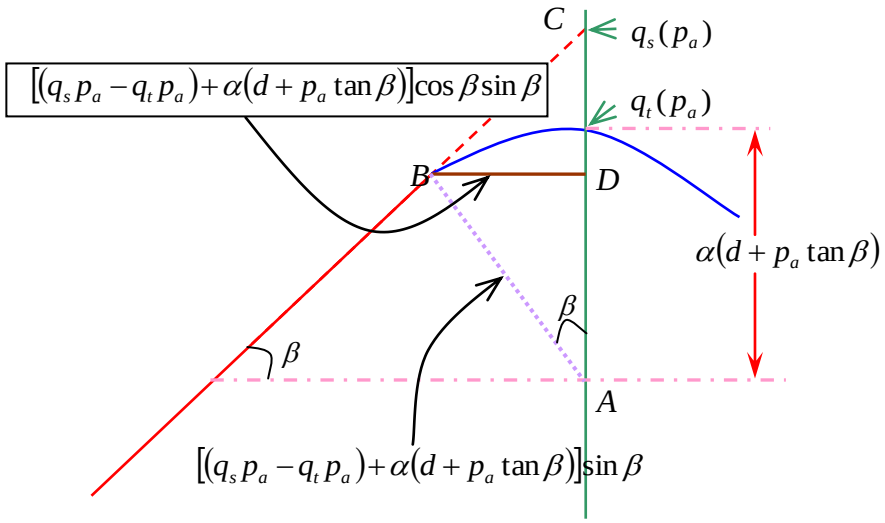

Fig.8: The range of transition surface in the modify Drucker Prager cap model.

Fig.9 and Fig.10 highlights the variable nature of the yield surfaces which change its shape and expand during compaction (increasing the extent of the elastic region inside the new yield surface). For powders, the position of the pressure yield surface depends on the density and generally achieves a higher level as densification of the powder takes place. This is referred to as hardening since the powder becomes harder to yield as it becomes more dense.

Kim et al. [14] verified that the Young's Modulus, E, and Poisson's ratio, ν, are functions of density, such that:

$$E = E_o \exp\left[-(b(1-D) + c(1-D)^2)\right] \tag{18}$$

$$\nu = \frac{1}{4}\left[\frac{3(1-\nu_o) + (7\nu_o - 3)D}{3(1-\nu_o) + (3\nu_o - 2)D}\right] \tag{19}$$

where $E_o = 406\,\text{GPa}$ and $\nu_o = 0.27$ are the respective bulk properties, D is the relative density of the compact, $b = 4.938$ and $c = 8.9438$ are curve fit parameters; The values of these parameters are obtained by fitting the experimental data found by others [16,21].

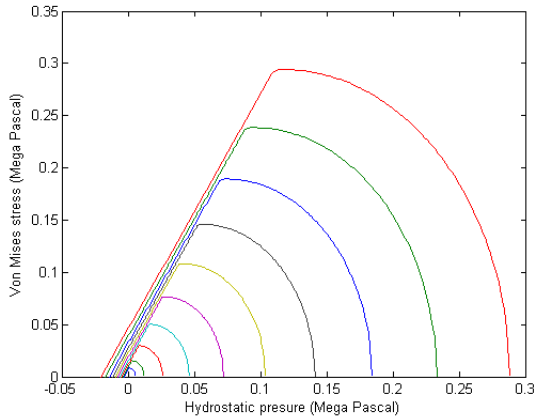

Fig.9: Yield Surfaces of alumina powder in the range of relative density $D:[0.42122,0.54984]$

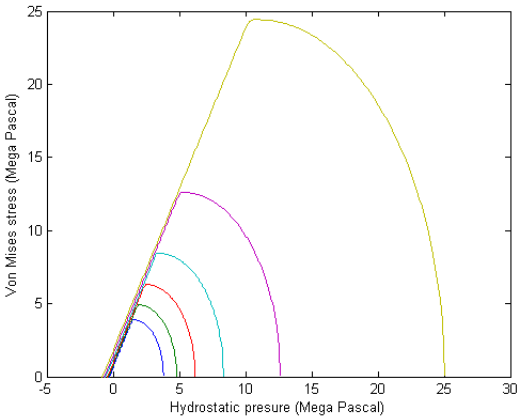

Fig.10: Yield Surfaces of alumina powder in the range of relative density $D:[0.83566,0.97856]$

Many numerical simulations are consider the Young's modulus and the Poisson's ratio as a constant during the process of compaction, while the experimental data shows they are depending on the density of the compact, by considering this approach, the properties of the powder will be more realistic, so it was adopted in this study.

The variation of the Young's modulus and the Poisson's ratio with relative density for an alumina powder compact, are shown in Fig.11 and Fig.12 respectively. It is clear that the Young's modulus and Poisson's ratio have to be updated depending on the relative density of the compact.

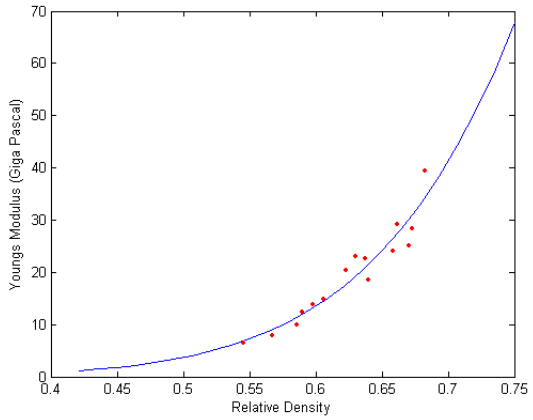

Fig.11: Variation of the Young's modulus with relative density for an alumina powder compaction.

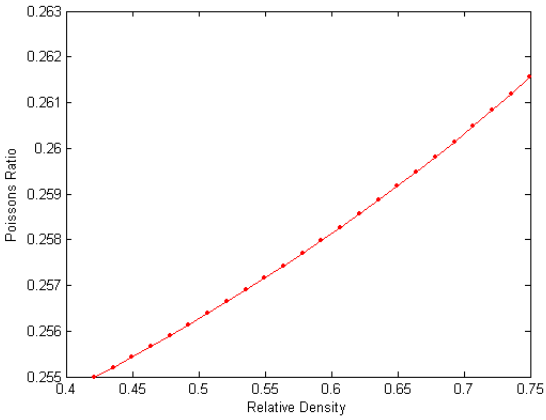

Fig.12: Poisson's ratio as a function of relative density for an alumina powder.

Computational Model:

An axisymmetric finite element model is created in ABAQUS version 6.4, to simulate densification of alumina powder under cold die pressing. Finite element results were compared with experimental data for density distribution of compact.

In this study the third deviatoric invariant r is not taken in to account i.e. $\tau = q$, requiring $K = 1$ in the equation (20) which is define a deviatoric stress measure in linear Drucker-Prager shear failure criterion:

$$\tau = \frac{q}{2}\left[1 + \frac{1}{K} - \left(1 - \frac{1}{K}\right)\left(\frac{r}{q}\right)^3\right] \qquad (20)$$

where K is a material parameter that represents the ratio of the distance of stress points on the tensile and compressive meridian from the hydrostatic axis in a specific deviatoric plane of the yield surface.

The material parameter which are used in compaction simulation are; material cohesion (8770-1.37E+06), angle of friction (66.269-65.581), cap eccentrivity (=0.558), yield stress (1893.7-1.00E+07), Young's modules (1.16E+09-2.85E+11), Poisson's ratio (0.255-0.267), and volumetric plastic strain (0-0.798) as a function of density in the range (1.679-3.73 gm/cm^3). The other parameters are chosen as, transition surface rate (=0.03), flow stress ratio (=1), initial yield surface position (=0).

Friction coefficients between powder and die are needed for the simulation. Usually, Coulomb type friction laws are used, yet other relations like the Tresca law, which relates the shear frictional stress with the shear yield strength of the compact, were also applied [20]. The value of 0.2 has been used in this work for verification and simulation purposes. The same friction coefficient was used between the powder and die and between the powder and punches.

The typical sample which used in this study is shown in Fig.13, the powder is surrounded by the die with a cylindrical shape. Correspondingly, a cylindrical shaped powder sample forms after the compaction. There are two punches acting on the top and bottom of the powder sample. One can assert a downward load on the top punch or an upward load on the bottom punch.

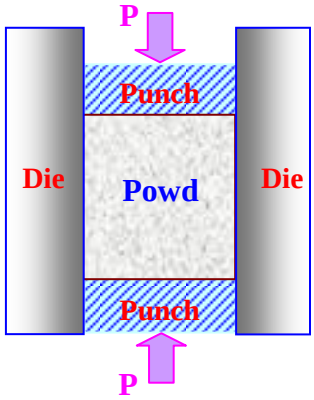

Fig.13: Cylindrical sample apparatus for compaction.

Single Acting Compaction Prediction:

Due to the axisymmetric nature of the compaction process, it was thus only necessary to consider half of the vertical cross section.

The powder was considered as deformable material, whereas the die wall and punches was modeled as a discrete rigid surface. The uniformed finite element mesh of 95 four-node axisymmetric elements CAX4R, and 120 nodes are considered, and 30 two-node axisymmitric rigid surface element RAX2 were used for die wall and punches.

The initial height of compacts $37.16mm$, diameter of compacts $20.2mm$, and the compacting pressure $38.6MPa$ was used [15]. The bottom of the material is immovable (fixed in both z- and r-directions) during compression, The top of the material moves vertically (in z-direction) downward during compression with velocity of $10\,mm/\min$, because of the action of top punch. The total amount of applied movement downwards, during compression, is the difference between the heights before compaction z_o, and at maximum applied stress $z_{\sigma\max}$. The nodes on the symmetrical axis were restricted to move in horizontal direction.

The interaction between the powder, die wall and punches were modeled by master-slave contacts with finite sliding. The Coulumbic friction coefficient, between the powder and tools was assumed to be constant, typically, a value of $\mu = 0.2$ was chosen. All thermal effects are considered to be negligible.

Ejection was simulated by sequentially releasing the surface boundary traction developed during pressing. The implementation of ejection was first applied by removing the upper boundary condition (unloading) after the completion of the pressing. Hence, the compact become free to relax in the z-direction while the compact was still in the die. The removal of the bottom boundary condition and the die wall (ejection) followed as the last step. Finally, the deformed structure (green component) was obtained.

The density distribution contour plots of the green alumina compact after the ejection, calculated by the finite element analysis, are presented in Fig.14, density is highest at the corner of contact surface between the upper punch and the die wall and lowest at the corner of contact surface between the lower punch and the die wall. A comparison of the experimental and theoretical density distribution shows that there is a good qualitative agreement in the sense that both produce the important maximum and minimum density regions accurately, despite the overall density distribution of present work is slightly underestimated experimental data.

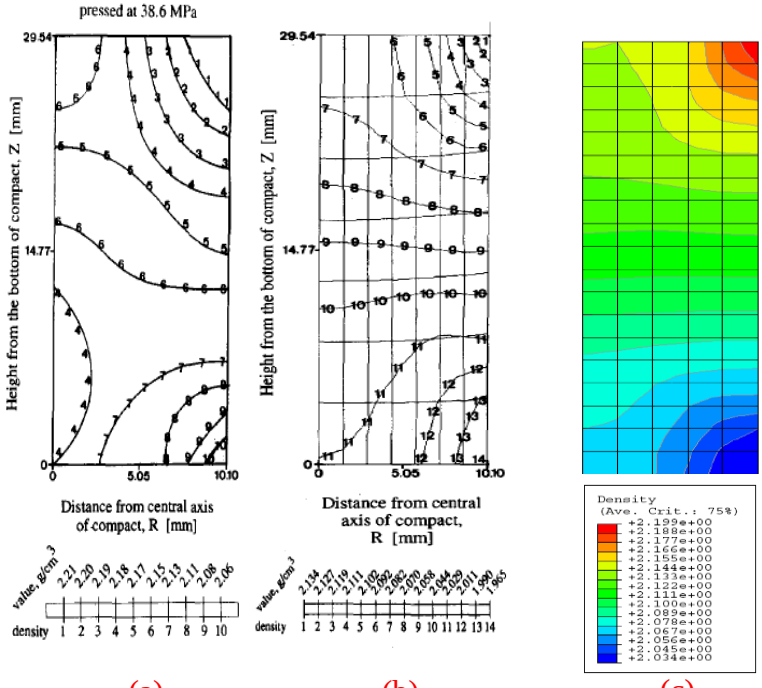

(a) (b) (c)

Fig.14: Comparison between experimental data and finite element result for the relative density distribution of the alumina powder compact after ejection under cold compaction: a.Experiment; b.FEM by Aydin et all[15], and c.Present work.

A first order comparison of the experimental and numerical density variation data is provided, at the locations of the wall and the symmetry axis, from the bottom to top of the cylindrical sample, at the wall of the cylindrical alumina compact, the density increases from the bottom, along the axial direction, in both experimental and numerical results as shown in Fig.15(a), the data are quite similar. The differences between the experimental and present numerical density data at top and bottom edges are -0.395% and -1.256% respectively.

Along the central line, however, axial density varies in a subtle way in the experimental data, while it simply increases towards the top in the numerical calculations as shown in Fig.15(b). The region of low density, on the centre line, at the bottom was predicted by present model with a difference of -5.099% from that of the experiments, and the region of low density on the tope are predicted with difference -0.218%.

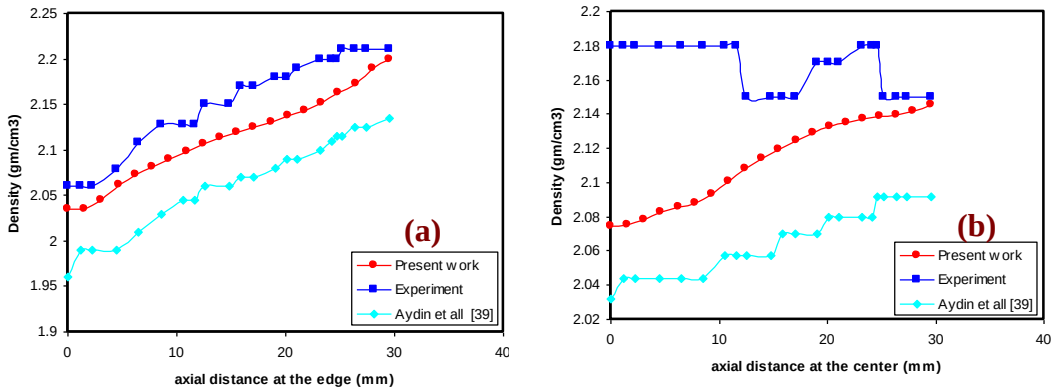

Fig.15: Comparison of the experimental and numerical density variation data; (a) at the locations of edge of compact; and (b) at the locations of centre of compact

Fig.16 shows the axial and radial contour displacements. The axial displacement decreases from the top of the bed to the bottom, showing that the axial load is transmitted from the upper layers to the lower ones. The radial contour displacements shows two distinct parts: an outwards flow at the top and an inwards flow at the bottom, between these parts, the material remains at the same radius. However, the magnitude of the radial displacement remains low compared to the axial displacement. Michrafy et al [22] founds the same behaviors in their numerical modeling for compaction the pharmaceutical powders.

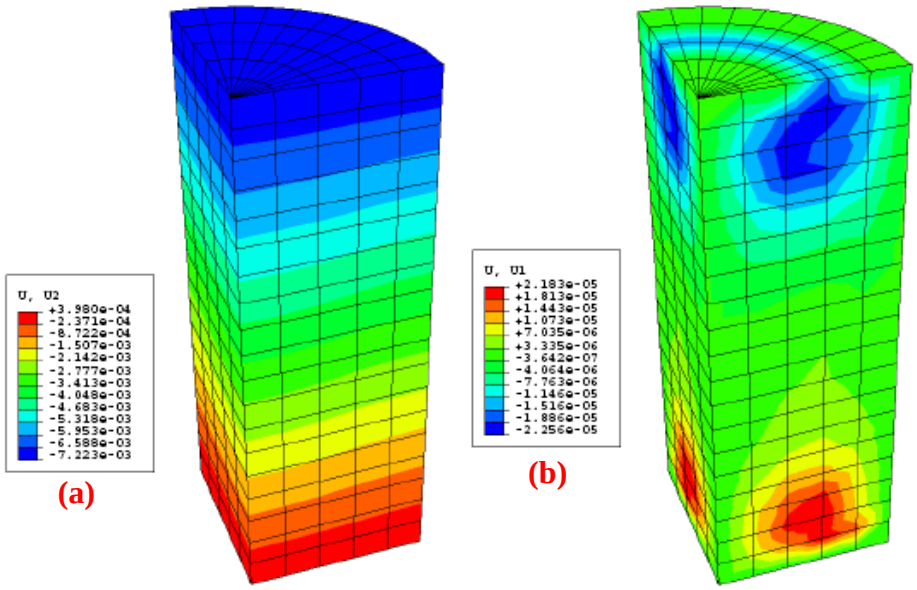

Fig.16: Control plot of: (a) axial and (b) radial displacements.

Conclusions:

For powders, the position of the pressure yield surface depends on the density and generally achieves a higher level as densification of the powder takes place, so that the Young's modulus and Poisson's ratio have to be updated depending on the relative density of the compact.

A comparison of the experimental and theoretical density distribution shows that there is a good qualitative agreement in the sense that both product the important maximum and minimum density regions accurately.

References:

[1] J. Mackerle, "Finite Element Analysis and Simulation of Powder Materials, Metallurgical Processes and Products, a Biblography 1985-2000", Journal of Materials Processing Technology, 133, 378-397, (2003).

[2] O. Coube, H. Riedel and T. Kraft, "Better Density Homogeneity and Reduced Warpage by Numerical Simulation of Die Pressing and Sintering", Powder Metallurgy World Congress 2000, K. Kosuge, H. Nagai (eds.), Japan Society of Powder and Powder Metallurgy, 1, 636-638, (2000).

[3] T. Kraft, H. Riedel, P. Stingl, and F. Wittig, "Finite Element Simulation of Die Pressing and Sintering", Advanced Engineering Materials, 1, (2), 107-109, (1999).

[4] T. Kraft, O. Coube, and H. Riedel, "Numerical Simulation of Pressing and Sintering in the Ceramic and Hard Metal Industry", NATO Advanced Research Workshop, Series III: Computer and Systems Science, 176, IOS Press, Amsterdam, Netherlands, 181-190, (2001).

[5] Hibbitt, Karlsson and Sorensen, Abaqus Theory Manual Version 6.4-1, Rhode Island: Hibbitt, Karlsson and Sorensen, Inc., (2003).

[6] T. Kraft, "Optimizing Press Tool Shapes by Numerical Simulation of Compaction and Sintering Application to a Hard Metal Cutting Insert", Modelling Simul. Mater. Sci. Eng., 11, 381–400, (2003).

[7] A. Schofield, and P. Wroth, "Critical State Soil Mechanics", London: McGraw Hill, (1968).
[8] M. Gasik, and B. Zhang, "A Constitutive Model and FE Simulation for the Sintering Process of Powder Compacts", Computational Materials Science, 18, 93-101, (2000).
[9] W. F. Chen, "Chapter 5: Constitutive Relations for Concrete, Rock and Soils: Discusser's Report, Section II", Mechanics of Geomaterials: Rocks, Concrete, Soils, ed. Z. P. Bazant, Chichester: John Wiley & Sons Ltd, 74-86, (1984).
[10] C. K. Kok, "Finite Element Simulations of Ceramic Powder Compaction and Sintering in the Making of a Micro Heat Exchanger", PhD Thesis, Michigan State University, (2004).
[11] I. Aydin, B. J. Briscoe and N. Ozkan, "Modeling of Powder Compaction: A Review", MRS Bulletin, 22, 45-51, (1997).
[12] D. C. Drucker, and W. Prager, "Soil Mechanics and Plastic Analysis or Limit Design", Quarterly of Applied Mathematics, 10, (2), 157-165, (1952).
[13] W. Wang, "Numerical Modeling of Compaction of Particulate Systems", MSc. Thesis, University of Florida, (1999).
[14] K. T. Kim, S. W. Choi and H. Park, "Densification Behavior of Ceramic Powder under Cold Compaction", Journal of Engineering Materials and Technology, 122, (2), 238-244, (2000).
[15] I. Aydin, B. J. Briscoe, and K. Y. Sanliturk, "Density Distributions During the Compaction of Alumina Powders: A Comparison of a Computational Prediction with Experiment", Computational Materials Science, 3, 55-68, (1994).
[16] H. G. Kim, O. Gillia, P. Doremus, and D. Bouvard, "Near Net Shape Processing of a Sintered Alumina Component: Adjustment of Pressing Parameters Through Finite Element Simulation", International Journal of Mechanical Sciences, 44, 2523-2539, (2002).
[17] O. Coube, and H. Riedel, "Numerical Simulation of Metal Powder Die Compaction with Special Consideration of Cracking", Powder Metallurgy, 43, (2), 123-131, (2000).
[18] S. Shima, and K. Mimura, "Densification Behavior of Ceramic Powder", International Journal of Mechanical Sciences, 28, (1), 53-59, (1986).
[19] T. Kraft, H. Riedel, and O. Rosenfelder, "Compaction and Sintering of a Ceramic Seal: Modeling and Experimental Response", Int. J. Powder Metall., 39, 27-34, (2003).
[20] H. Riedel and T. Kraft, "Chapter 26: Simulation in Powder Technology", Continuum Scale Simulation of Engineering Materials: Fundamentals – Microstructures – Process Applications. Edited by Dierk Raabe, Franz Roters, Frederic Barlat, Long-Qing Chen, Wiley-VCH Verlag GmbH & Co. KGaA, (2004).
[21] Y. Y. Foo, Y. Sheng, and B. J. Briscoe, "An Experimental and Numerical Study of the Compaction of Alumina Agglomerates", International Journal of Solids and Structures, 41, 5929-5943, (2004).
[22] A. Michrafy, D. Ringenbacher, and P. Tchoreloff, "Modelling the Compaction behaviour of Powders: Application to Pharmaceutical Powder", Powder Technology, 127, 257-266, (2002).

دراسة محاكاة لعملية تشكيل المسحوق السيراميكي

نوميد غريب عبدالله [(*)]، **فاضل عبد رسن** [(**)]، **طارق عبد الرضا**[(***)]
[(*)] جامعة السليمانية، كلية العلوم، قسم الفيزياء
[(**)] جامعة المستنصرية، كلية العلوم، قسم الفيزياء
[(***)] جامعة بغداد، كلية التربية (ابن الهيثم)، قسم الفيزياء

الخلاصة

ان المحاكاة الدقيقة لعملية تشكيل المسحوق تقتضي العديد من المجالات ضمن الميكانيكا الحسابية، و منها على سبيل المثال نموذج مرن-لدن تركيبي ملائم، اطار التشوية المحدد، تاكيد على نقاط التماس، ظروف الاحتكاك، و طرق عددية قوية. تم في هذا البحث استخدام النموذج مرن-لدن DPC المعدل في الحسابات التي اجريت باستخدام برنامج العناصر المتناهية ABAQUS 6.4، لغرض محاكاة عملية تكثيف مسحوق اوكسيد الالمنيوم باستخدام الكبس البارد. بمقارنة التوزيعين التجريبي و النظري للكثافة تبين ان هناك اتفاقا جيدا بينهما، من حيث ان كليهما يعطي الحد الاعلى و الادنى للكثافة بدقة، بالرغم من ان النتائج المحصلة في بحثنا هذا هي اقل من بيانات تجريبية نوعا ما.